HHS Public Access

Author manuscript

Nat Neurosci. Author manuscript; available in PMC 2017 May 28.

Published in final edited form as:

Nat Neurosci. 2017 January ; 20(1): 24–33. doi:10.1038/nn.4449.

Mechanosensory hair cells express two molecularly distinct mechanotransduction channels

Zizhen Wu[#1], **Nicolas Grillet**[#2], **Bo Zhao**[3], **Christopher Cunningham**[1], **Sarah Harkins-Perry**[3], **Bertrand Coste**[4], **Sanjeev Ranade**[5], **Navid Zebarjadi**[2], **Maryline Beurg**[6], **Robert Fettiplace**[6], **Ardem Patapoutian**[5], and **Ulrich Mueller**[1]

[1]The Solomon Snyder Department of Neuroscience, Johns Hopkins University, Baltimore, Maryland USA

[2]Department of Otolaryngology – Head and Neck Surgery, Stanford University, Stanford, California, USA

[3]Department of Molecular and Cellular Neuroscience, The Scripps Research Institute, La Jolla, California, USA

[4]Aix-Marseille-Universite, CNRS, Marseille, France

[5]Howard Hughes Medical Institute, Department of Molecular and Cellular Neuroscience, The Scripps Research Institute, La Jolla, California, USA

[6]Department of Neuroscience, University of Wisconsin Medical School, Madison, Wisconsin, USA

[#] These authors contributed equally to this work.

Abstract

Auditory hair cells contain mechanotransduction channels that rapidly open in response to sound-induced vibrations. Surprisingly, we report here that auditory hair cells contain two molecularly distinct mechanotransduction channels. One ion channel is activated by sound and is responsible for sensory transduction. This sensory transduction channel is expressed in hair-cell stereocilia and previous studies show that its activity is affected by mutations in the genes encoding the

Corresponding Author, Ulrich Müller, Solomon Snyder Department of Neuroscience, Johns Hopkins Medical Institute, 725 N. Wolfe Street, Baltimore, MD 21209, USA, P:443-287-4762, umuelle3@jhmi.edu.

ACCESSION CODES

Not applicable.

DATA AVAILABILITY STATEMENT

The data that support the findings of this study are available from the corresponding author upon reasonable request.

AUTHOR CONTRIBUTIONS

All authors contributed to experimental design. Z.W. and N.G. designed and performed most of the experiments. S.R. generated some of the genetically modified mice, C.C. and N.Z. participated in gene expression studies, B.Z. carried out electron microscopic studies, B.C. analyzed effects of pharmacological inhibitors on Piezo2 expressed in heterologous cells, S.H.-P. carried out ABR/DPOAE recordings and participated in the generation of genetically modified mice, and M.B. analyzed effects of calcium on mechanotransduction. U.M., A.P. and R.F. supervised the experiments and participated in data analysis and interpretation. U.M. and Z.W. wrote the manuscript with significant input from the other authors.

COMPETING FINANCIAL INTEREST STATEMENT

Ulrich Müller is a co-founder of Decibel Therapeutics.

transmembrane proteins TMHS/LHFPL5, TMIE and TMC1/2. We show here that the second ion channel is expressed at the apical surface of hair cells and contains the Piezo2 protein. The activity of the Piezo2-dependent channel is controlled by the intracellular Ca^{2+} concentration and can be recorded following disruption of the sensory transduction machinery or more generally by disruption of the sensory epithelium. We thus conclude that hair cells express two molecularly and functionally distinct mechanotransduction channels with different subcellular distribution.

INTRODUCTION

Our senses of hearing, balance, proprioception and touch depends on the conversion of mechanical force into electrical signals. The molecules underlying mechanoelectrical transduction are not well defined and the extent to which different mechanosensory phenomena depend on similar molecules to convert mechanical into electrical signals still needs to be defined. In the organ of Corti of the mammalian cochlea (Fig. 1A) hair cells are the mechanosensory cells for the perception of sound. Mechanotransduction channels in hair cells are localized in their hair bundles, which consist of stereocilia that are organized in rows of decreasing heights (Fig. 1B)[1]. In a healthy hair cell, deflection of the hair bundle towards the longest stereocilia leads to an increase in the open probability of transduction channels, while deflections in the opposite direction decrease channel open probability[1]. Mechanotransduction channels are gated by tip links, the extracellular filaments that connect the stereocilia of a hair cell in the direction of the mechanical sensitivity of its hair bundle (Fig. 1B)[1].

There is considerable uncertainty with regard to the molecular composition of the mechanotransduction channel in hair cells. Ca^{2+} enters stereocilia upon mechanical stimulation near the lower tip-link insertion site, thus defining the localization of the sensory transduction channel[2]. TMHS/LHFPL5, TMIE, TMC1 and TMC2 are transmembrane proteins that are appropriately localized in stereocilia to be part of a transduction-channel complex[3-5]. Which of these proteins contribute to the channel pore is unclear. Functional studies in mice suggest that TMHS/LHFPL5, a protein with four predicted transmembrane domains, is alone not a pore-forming subunit of the transduction channel but part of the channel complex[4]. TMIE contains two predicted transmembrane domains and is essential for mechanotransduction by hair cells but its precise function within the transduction-channel complex remains to be established[5]. TMC1 and TMC2 contain at least six predicted transmembrane domains[6] and have been proposed to be components of the mechanotransduction channel[7, 8], possibly forming its pore[9]. However, it has so far not been possible to demonstrate that TMC1 and/or TMC2 encode ion channels.

During the developmental maturation of hair cells, their hair bundles are less directionally sensitive; transducer currents can initially be evoked by deflection of the hair bundle in the opposite from normal direction[10-13]. Similar reverse polarity currents can be evoked in hair cells lacking tip links[10, 12, 14] and in hair cells from mice carrying mutations in the genes encoding TMHS/LHFPL5, TMIE, and TMC1/2[5, 10, 15]. Appearance of reverse-polarity currents in damaged hair cells correlates with loss of normal-polarity currents suggesting that the pore-forming subunits of the underlying ion channels may be shared. Consistent

with this notion, ion channels carrying reverse-polarity currents show similar but not identical ion selectivity and responsiveness to pharmacological blockers as ion channels for normal-polarity currents[8, 10, 16]. Based on these and other findings, it has been proposed that TMC1/2 might be accessory subunits of the transduction channel that regulate channel localization and/or form an extracellular vestibule that controls ion flow towards the channel pore[8, 10, 15-17].

Recent findings have identified Piezo1 and Piezo2 proteins as bona-fide pore-forming subunits of mechanotransduction channels in mammals[18, 19]. Piezo proteins have important functions in touch sensation and other mechanical processes such as the sensing of shear stress in the vasculature and the regulation of bladder function[20]. However, the function of Piezo1 and Piezo2 in auditory hair cells has not been thoroughly explored. Here we show that Piezo2 is expressed in cochlear and vestibular hair cells. Studies in cochlear outer hair cells (OHCs) show that Piezo2 is not an essential component of the sensory transduction channel in stereocilia. Instead, Piezo2 is localized apically within the hair cell body and required for the reverse polarity currents that are observed during hair cell development, after tip-link breakage, and in hair cells lacking TMC1/2. Piezo2 function is controlled by the intracellular Ca^{2+} concentration suggesting that the two Ca^{2+}-permeable ion channels responsible for the forward and reverse polarity currents might engage in regulatory cross-talk. We thus conclude that hair cells contain two moleculary distinct mechanotranduction channels with different subcellular distribution and function. While Piezo2 is likely a pore-forming subunit of the reverse-polarity channel in hair cells, the proteins that form the pore carrying the normal-polarity sensory transduction current still need to be determined. Overall, our findings show that mechanically gated ion channels important for different sensory modalities such as for the perception of touch and sound depend at least in part on different molecular components.

RESULTS

Piezo2 is expressed in OHCs of the cochlea and in vestibular hair cells

To determine the expression patterns of *Piezo1* and *Piezo2* in the inner ear, we carried out in situ hybridization in sagittal sections of the murine cochlea at postnatal day (P) 1 using antisense and control sense probes (Fig. 1C). As a positive control, we used a probe for *otoferlin*, which highlights both IHCs and OHCs at this age (Fig. 1C)[21, 22]. We did not detect significant levels of *Piezo1* mRNA in the inner ear. In contrast, *Piezo2* expression was detected at low amounts in the cytoplasm of OHCs between the cell nucleus and the cuticular plate (Fig. 1C).

To confirm the expression pattern of *Piezo2* in the inner ear, we crossed *Piezo2-GFP-IRES-Cre* mice expressing a *Cre* transgene from the endogenous *Piezo2* genetic locus[23] with the *Ai9* mouse line, a Cre-dependent *td-Tomato* reporter[24]. In cochlear whole mounts at P7, *td-Tomato* expression was detected in OHCs throughout the length of the cochlear duct (Fig. 1D-G,I). We rarely observed Piezo2 expression in IHC but they may express low levels of Piezo2 that were hard to detect (Fig. 1E,G,I; arrowheads). We also observed *td-Tomato* expression in blood vessels. This was particularly obvious at P0 when expression levels of the fluorescence reporter in hair cells were less prominent (Fig. 1H). Analysis of the

vestibule similarly revealed expression in hair cells (Fig. 1J-O; arrowhead) and blood vessels (Fig. 1J-O).

Analysis of brain sections of mice obtained by crossing *Piezo2-GFP-IRES-Cre* mice with *Ai9* mice revealed Piezo2 expression in blood vessels (Supplementary Fig. 1) but not in neurons throughout the auditory pathway, including neurons of the cochlear nucleus and superior olivary nucleus (Supplementary Fig. 1). Similar observations were made when we analyzed Piezo2 expression by in situ hybridization (not shown).

Hearing function in *Piezo1/2*-deficient mice

To determine the function of Piezo proteins in the inner ear, we crossed *Piezo2-flox* mice[23] with *Pax2-Cre* mice, which express Cre in the presumptive otic ectoderm thus leading to inactivation of *Piezo2* throughout the inner ear[25-28] (*Pax2* is also expressed in midbrain neurons[29], but we did not observe Piezo2 expression in midbrain neurons; Supplementary Fig. 1). While we did not observe *Piezo1* expression in the inner ear, we also inactivated *Piezo1* expression in combination with *Piezo2* by crossing *Piezo1-flox;Piezo2-flox* mice with *Pax2-Cre* mice. We will refer to the mutant mice in the following as *Piezo2cko* mice, and *Piezo1/2dcko* mice. For some experiments we inactivated *Piezo1* alone by crossing *Piezo1-flox*[30] mice with *Pax2-Cre* and we will refer to the mutant mice as *Piezo1cko* mice.

Measurement of the auditory brain stem response (ABR) to broadband click-stimuli at P60 revealed a slight elevation (~15dB) of auditory thresholds in *Piezo2cko* and *Piezo1/2dcko* mice relative to control wild-type and *Pax2-Cre* mice (Fig. 2A,B). Similar observations were made for pure tones between 8 and 20 kHz (Fig. 2C). Above 20 kHz, *Pax2-Cre* mice showed elevated thresholds compared to wild-type (Fig. 2C), suggesting that the genetic background of the Cre mouse line mildly affect auditory function at higher frequencies preventing the analysis of Piezo1/2 function above 20 kHz.

We next recorded distortion product otoacoustic emissions (DPOAEs), which are mechanical distortions generated in the inner ear when two primary tones (f_1 and f_2) are presented. Outer hair cells (OHCs) amplify the distortions, which are propagated back through the middle ear and ear canal and can be measured in sound pressure waveforms. We determined signals above the noise floor at the 2f1-f2 frequency. Signals of 10 dB or greater above the noise level were scored as a positive signal. DPOAEs in *Piezo2cko* and *Piezo1/2dcko* mice were elevated between 8 and 20 kHz (Fig. 2D), which is consistent with the ABR data. We thus conclude that OHC function is mildly affected in *Piezo2cko* mice.

Piezo2cko and *Piezo1/2dcko* mice did not show obvious vestibular defects, which frequently manifest in mice by abnormal head posture and circling behavior. For quantification, we analyzed vestibular function in swim tests scoring tail activity, hind leg activity, head position and body posture as described[31]. We did not observe any measurable defects between wild-types and mutants (Supplementary Fig. 2). Given the mild auditory defects and lack of obvious vestibular defect, we did not evaluate vestibular function by electrophysiology.

Piezo2 localization in hair cells

To further define the function of Piezo1 and Piezo2 in hair cells and to confirm efficient ablation of Piezo1/2 proteins in the inner ear of mutant mice, we stained cochlear whole mounts with phalloidin to reveal their F-actin cytoskeleton and with antibodies to Piezo1 and Piezo2[23, 30]. We used identical exposure times to collect images from wild-type and mutant animals. Consistent with our in situ hybridization data, we did not observe Piezo1 expression in the inner ear (not shown). In contrast, cochlear whole-mount staining for Piezo2 revealed expression in OHCs at P5 (Fig. 3A-C). No expression was observed in *Piezo2cko* mice, confirming the specificity of the staining signal (Fig. 3B). To analyze Piezo2 localization in hair cells more precisely, we collected optical sections from the tops of the stereocilia to the bottom of the hair-cell body (Fig. 3B,C). Piezo2 expression was detected near the apical surface of the cell body of hair cells where it appeared to be most concentrated close to the adherens junctions near the longest stereocilia (Fig. 3B,C,D). Piezo2 expression was not detected within the stereocilia, and very low amounts if any were observed along the lateral membrane between hair cells and support cells (Fig. 3B). We collected higher magnification images and increased the exposure time dramatically but could not detect Piezo2 in stereocilia, while it was clearly detected near the apical surface of hair cells (Fig. 3C). We conclude that Piezo2 is probably not appropriately localized to be a component of the sensory transduction channel that is present in hair-cell stereocilia near tip links[2].

Hair cell electromotility

The expression of Piezo2 in OHCs promted us to investigate its role in amplification. Amplification by OHCs depends on length changes of the cell bodies of OHCs termed electromotility. Electromotility is accompanied by a voltage-dependent gating charge movement within the lateral membrane of OHCs, manifesting as a nonlinear capacitance[32-35]. Measurements of the nonlinear capacitance at P15 did not reveal significant difference between OHCs from wild-type and *Piezo2cko* mice (Supplementary Fig. 3). We conclude that Piezo2 is likely not essential for normal amplification by OHCs.

Hair bundle morphology and mechanotransduction

We next asked whether Piezo2 might have a function in hair bundle development. We stained cochlear whole mounts at P80 with phalloidin but observed no obvious morphological defects in hair bundles or in the patterning of the sensory epithelium into three rows of OHCs and one row of IHCs (Fig. 4A,B). Similar observations were made at P5 (Fig. 3B). The findings were confirmed by scanning electron microscopy (SEM) at P5 (Fig. 4C-L). Bundle polarity was maintained, hair cells formed a normal stair-case and they were connected by filamentous linkages (Fig. 4M,N).

Although we did not detect Piezo2 expression in hair cell stereocilia, OHC function is mildly affected in *Piezo2cko* mice (Fig. 2). We thus analyzed the extent to which mechanotransduction was affected in hair cells from *Piezo1/2dcko* mice. We stimulated hair bundles of OHCs at P7 with a stiff glass probe (Fig. 5A) and recorded mechanotransduction currents in the whole-cell configuration. As reported[4, 5, 36], OHCs from control mice had rapidly activating transducer currents, which subsequently adapted (Fig. 5A). Current

displacement plots did not reveal an obvious difference in transducer current in hair cells from controls and *Piezo1/2dcko* mice (Fig. 5B). The amplitude of saturated mechanotransduction currents in hair cells in the mid-apical part of the cochlea at maximal deflection with a stiff glass probe was at 498.47 ± 35.99 pA (mean ± SEM) for control OHCs and 498.03 ± 54.19 pA (mean ± SEM) for OHCs from mutants (Fig. 5B).

Severe defects in stiffness of hair bundles manifest as defects in mechanotransduction when hair bundles are stimulated with a fluid jet. We have conducted the fluid jet experiments at P7 but did not observe significant differences between OHCs from wild-type and mutants (Supplementary Fig. 4).

Reverse-polarity currents in *Piezo1* and *Piezo2* single and double mutants

The reverse-polarity current that was originally reported for OHCs shows similar kinetic properties with rapid onset followed by rapid adaptation as observed for Piezo2[10, 18]. We thus tested the extent to which the reverse-polarity current was dependent on Piezo2. For this purpose, we used the fluid-jet stimulation system that has previously been used to deflect hair bundles in the normal-polarity and reverse-polarity direction[5, 10]. The experiments were carried out with 99 OHCs from 39 pups at P5. We recorded regular normal-polarity currents in hair cells from control, *Piezo1cko, Piezo2cko* and *Piezo1/2dcko* mice (Fig. 5A-C, data not shown). Robust reverse-polarity currents were also recorded in OHCs from control and *Piezo1cko* mice following the disruption of tip links with 5 mM BAPTA (Fig. 5C-F). However, no reverse-polarity currents could be evoked in the vast majority of OHCs from *Piezo2cko* and *Piezo1/2dcko* mice after tip-link disruption (Fig. 5C-F). The few hair cells that showed reverse-polarity currents might be a small population of OHCs that did not efficiently express Cre used to inactivate *Piezo1* and *Piezo2*. It is also formally possible that another channel is responsible for these rare reverse-polarity currents.

We next evaluated the extent to which Piezo2 expressed in heterologous cells and the reverse polarity current in hair cells was sensitive to dihydrostreptomycin (DHS). Previous studies have established for the reverse polarity channel a 30 percent block by 100 μM DHS in 1.5 mM extracellular Ca^{2+} [16]. We now show that 100 μM DHS gives 40 percent and 25 percent block of Piezo2 expressed in HEK cells (Supplementary Fig. 5) at an extracellular Ca^{2+} concentration of 100 μM and 2.5 mM, respectively.

We were unable to induce reverse-polarity currents in the majority of P5 IHCs both in wild-type mice following disruption of tip links and in TMC1/2 double mutants (Fig. 5G,H), which is consistent with the observation that we rarely observe *Piezo2* expression in IHCs.

Effects of intracellular Ca^{2+} concentration on reverse-polarity currents

The appearance of reverse-polarity currents correlates with the disappearance of normal-polarity currents, which has led to the hypothesis that the two currents might depend on similar pore-forming ion-channel subunits[10, 15, 16, 37]. Since our data suggest that different ion channels carry reverse-polarity and normal-polarity currents, we asked whether ion channels carrying normal-polarity currents suppress the activity of ion channels responsible for reverse-polarity currents. Significantly, transduction channels in OHCs are not completely closed at rest and the intracellular Ca^{2+} concentration in OHCs is high[17, 38-40].

Channels close after tip-link breakage thus preventing influx of Ca^{2+} through transduction channels[41]. We therefore tested the extent to which the intracellular Ca^{2+} concentration might affect reverse-polarity currents.

The reverse-polarity current was suppressed by elevating the intracellular Ca^{2+} concentration. This is exemplified by MT currents in early post-natal mice (Fig. 6A; P0 basal OHCs) in which the hair cells displayed normal- and reverse-polarity currents when recordings were made with a patch pipette containing a solution that included the Ca^{2+} buffer EGTA (Fig.6A). However, if recordings were made in the same preparation using an intracellular solution containing 1 mM Ca^{2+}, the reverse polarity current was present immediately after rupturing the patch but quickly disappeared as the high Ca^{2+} washed into the cytoplasm (Fig. 6B). There was no significant reduction in the amplitude of the normal MT current (Fig. 6B), indicating no general deterioration in the cell during perfusion with high Ca^{2+}. Similar effects of Ca^{2+} wash-in were seen in five OHCs with 1 mM Ca^{2+} in the pipette solution; in these cells the mean reverse-polarity current was 600 ± 130 pA immediately after attaining whole-cell and diminished after four minutes recording to 2 ± 0 pA. If 0.1 mM Ca^{2+} was present in the patch-pipette solution, the reverse-polarity current was unaffected after 14 min of recording. A similar Ca^{2+} block was obtained if the reverse-polarity current was elicited in *Tmc1:Tmc2* double knockouts or after destruction of the tip links by exposing the hair bundle to BAPTA (not shown).

The Ca^{2+} concentration needed to suppress the reverse-polarity current is high but not unrealistic since we have previously estimated from Ca^{2+} reversal potential measurements that the Ca^{2+} in the stereocilia is near a millimolar concentration[17]. While the Ca^{2+} concentration is likely highest near the inner face of the MET channel, the concentration further down the stereocilium and at the top of the cell will still be significant as Ca^{2+} buffering in neonates is small[42]. Furthermore, the GHK equation used to infer the Ca^{2+} level[17] applies to the bulk concentration just as the membrane potential refers to the potential difference between the bulk solutions, not the membrane surface potential. During neonatal development, Ca^{2+} influx through the normal MT channels (which are two to three times more Ca^{2+}-permeable than the reverse-polarity ones; see Beurg et al., 2014) therefore likely increases Ca^{2+} to a level sufficient to suppress the reverse-polarity current.

We next tested the extent to which the intracellular Ca^{2+} concentration affects Piezo2 function directly. We expressed Piezo2 in HEK293 cells and applied a series of force steps to the cell surface via a piezo-driven glass probe. Currents were recorded with whole-cell voltage clamp recordings with a pipette solution containing up to 10 mM Ca^{2+}. There was no obvious effect of Ca^{2+} on the maximal response of Piezo2 to mechanical stimulation even after minutes of perfusion (Fig. 6C). These data suggest that Ca^{2+} affects Piezo2 indirectly, perhaps by regulating the activity of other proteins such as a kinase, which then regulates Piezo2 function or transport directly or via Piezo2-associated proteins. This interpretation is consistent with the observation that it takes minutes for reverse polarity currents to reach full amplitude following disruption of tip links[10].

Maturation of normal-polarity currents

All recordings described so far were carried out with hair cells from mice where Piezo2 function was inactivated by tissue-specific Cre-mediated recombination. Although our immunolocalization studies suggested that we efficiently inactivated Piezo2 function in *Piezo2cko* mice (Fig. 3), we wanted to exclude that a small amount of Piezo2 protein might have persisted. We therefore analyzed transducer currents in hair cells from *Piezo2-null* mice. Since *Piezo2-null* mice die at birth[43], we established cochlear cultures from mice at E18.5 and cultured them for several days. We stimulated OHCs from wild-type and mutants at a similar position in the medial part of the cochlea with a fluid jet, which allowed us to record forward-polarity and reverse-polarity currents. As reported earlier in rat[13] and mice[10, 37, 44], transducer currents in wild-type mice matured in vitro over several days (Fig. 7A). Similar to previous reports using zebrafish and rodents[10-13, 37] we observed that currents in immature hair cells of wild-type mice at P0 revealed both normal- and reverse-polarity currents with normal-polarity currents not having reached full amplitude (Fig. 7A). In wild-type, the amplitude of normal-polarity currents increased nearly 8 fold after one day in culture and even further after two days (Fig. 7A), which is consistent with the progressive maturation of the transduction machinery even in vitro. In striking contrast, in OHCs from *Piezo2-null* mice, reverse polarity currents were not detectable at P0 or after culturing hair cells for one or two days (Fig. 7A). However, normal-polarity currents were present but they appeared to reach full amplitude on an accelerated time course. Normal-polarity currents were nearly 4-fold larger in mutants at P0 compared to wild-type, about 2-fold larger after 1 day in culture but indistinguishable from wild-type after 2-days in culture. A similar delay in maturation was observed with acutely isolated hair cells from *Piezo2cko* mice. In explants from *Piezo2cko* mice mechanotransduction currents at P0 were small and indistinguishable between wild-type and mutants but over the next 3 days they matured slightly faster in hair cells from *Piezo2cko* mice compared to wild-type (Fig. 7 B).

Induction of reverse-polarity currents by damage to the sensory epithelium

Disruption of tip links and genetic mutations that affect components of the sensory transduction machinery in stereocilia such as LHFPL5/TMHS, TMIE and TMC1/2 unmask reverse-polarity currents in hair cells[5, 10, 12, 15]. Reverse polarity currents were not induced by careful dissection of the sensory epithelium of wild-type mice for electrophysiological recordings (Fig. 5C). Treatment of organ explants with chemicals that cause oxidative stress such as H_2O_2 also did not lead to an activation of reverse-polarity currents (not shown). However, when we mechanically disrupted the integrity of the sensory epithelium with a pipette, robust reverse-polarity currents were evoked in OHCs (Fig. 7C) near the stab wound (<10 cell-diameters distance) but not further away (>20 cell-diameter distance) were epithelial architecture was not affected (Fig. 7C). Significantly, in hair cells near the stab wound, forward-polarity currents of normal amplitude and reverse-polarity currents could be evoked in parallel in the same cell (Fig. 7C). These findings suggest that reverse-polarity currents in OHCs can be evoked by mechanical damage to the sensory epithelium. Significantly, both the forward-polarity and reverse-polarity currents co-exist in the same cell within the damaged epithelium, which is consistent with the observation that the two currents depend on different ion channels.

DISCUSSION

We provide here evidence that OHCs in the murine cochlea express two molecularly and functionally distinct mechanotransduction channels. One transduction channel is present in the stereocilia near tip links and is required for sensory transduction. The second transduction channel contains Piezo2 and is concentrated at the apical surface of OHCs. The Piezo2-containing ion channel is observed in developing hair cells and can be unmasked at later developmental stages by breakage of tip links or by damage to the sensory epithelium. Intriguingly, auditory function is mildly perturbed in the absence of Piezo2. As one possibility, the mild auditory defects in *Piezo2cko* mice perhaps indicate a role for Piezo2 in facilitating continuous repair in the sensory transduction machinery, which might undergo turnover throughout life.

Hair cells of the mammalian cochlea are mechanosensory cells that convert sound-induced vibrations into electrochemical signals. The mechanically-gated ion channel that is activated by sound has been studied for decades[1]. This sensory transduction channel is activated by deflection of the hair bundle in the direction of the longest stereocilia (normal-polarity) and is present in stereocilia near the lower end of tip links. LHFPHL5, TMIE and TMC1/2 are candidate subunits of the sensory transduction channel[4, 5, 7, 9]. The observation that OHCs express a second mechanically activated ion channel at their apical surface is a surprise. We show that this ion channel contains Piezo2 and is activated in early developing hair cells by stimulation of the hair bundle in the opposite from normal direction (reverse-polarity). In wild-type hair cells, the sensory transduction machinery matures postnatally over several days[10, 13, 37, 44]. Surprisingly, our findings indicate that maturation is slightly accelerated in the absence of Piezo2. The mechanism by which Piezo2 affects the maturation of the sensory transduction machinery is unknown and the physiological relevance of the phenomenon needs further investigation. The observation that Ca^{2+} regulates the activity of the Piezo2-dependent ion channel and that Piezo2 in turn is permeable to Ca^{2+} raises the possibility that Ca^{2+} plays a role in the maturation process of the sensory transduction machinery (Fig. 7D).

Previous studies have shown that a reverse-polarity current can be evoked in postnatal cochlear hair cells following disruption of the sensory transduction machinery[5, 10, 12, 14, 15]. The reverse-polarity current has similar properties as the normal polarity current and it has been proposed that the two currents might be carried by similar pore-forming ion-channel subunit[10, 15, 16, 37]. Our findings suggest that different ion channels carry the forward-polarity and reverse-polarity currents, where only the reverse-polarity current depends on Piezo2. Significantly, the kinetic properties[10, 18] and pharmacology (sensitivity to DHS and FM1-43)[12, 16, 37, 45] of the reverse-polarity current resembles the properties of Piezo2, suggesting that Piezo2 forms the pore of the channel carrying the reverse-polarity current.

One previous study has reported that following the breakage of tip links, reverse-polarity currents can be observed in IHCs between P6-P9. These reverse polarity currents were more variable in size[12]. We report here that we rarely observed reverse polarity currents in IHCs at P4-P6 after tip-link breakage, which is consistent with our findings that we detected Piezo2 expression only in a subset of IHCs. The difference between the two studies might be

explained in several ways. First, expression levels of Piezo2 in IHCs might vary between mice of different genetic background. Second, hair cells might contain additional ion channels and variations in the stimulation protocol between laboratories might lead to the activation of different subsets of channels. Third, the published study[12] did not provide information on the number of IHCs that revealed a reverse-polarity current. Thus, it is possible that the previous study focused on the characterization of the limited number of IHCs that express Piezo2.

As reported earlier in rat[13] and mice[10, 37, 44] transducer currents in wild-type mice mature in vitro over several days. In addition, in zebrafish and rodents[10-13, 37] mechanically evoked currents in immature hair cells are less directionally sensitive revealing normal-polarity and reverse-polarity currents. During development, the reverse-polarity current declines while the normal polarity current matures and is detectable in both IHCs and OHCs[37]. These findings suggest that the reverse polarity currents recorded at earlier developmental time points in IHC might be carried by an ion channel distinct from Piezo2. In fact, it has been proposed that the reverse- and normal-polarity currents in developing hair cells might be carried by the sensory transduction channel in hair bundles that have not reached their normal polar arrangement of stereocilia[13]. Formally, we cannot exclude the possibility that Piezo2 might be expressed at very low levels in IHCs below the limit of detection by our methods.

We are intrigued by the observation that Ca^{2+} regulates the activity of the Piezo2-dependent ion channel. This observation perhaps explains why reverse-polarity currents are prominently detected in postnatal hair cells after but not before disruption of the sensory transduction machinery. Sensory transduction channels are not completely closed at rest leading to influx of Ca^{2+} [38]. The Ca^{2+} concentration in stereocilia in rodents has been estimated to be in the range of ~1 mM[17]. Upon disruption of the transduction machinery, intracellular Ca^{2+} levels decline, which could then lead to the activation of the Piezo2-dependent ion channel (Fig. 7D). Consistent with this model, when we increase intracellular Ca^{2+} levels in hair cells following tip-link breakage, the activity of the Piezo2-dependent ion channel is reduced. When we expressed Piezo2 in heterologous cells, we could not alter its activity by changes in the intracellular Ca^{2+} concentration. This suggests that the effect of intracellular Ca^{2+}-levels on Piezo2-function may be indirect (Fig. 7D). Consistent with this model, reverse-polarity currents of full amplitude are observed in hair cells only several minutes after disruption of tip links[10]. This could be in part attributed to slow changes in the intracellular Ca^{2+} concentration but might also signify intermediate steps in the regulation of Piezo2 function, for example by a Ca^{2+}-dependent kinase that phosphorylates Piezo2 directly or a Piezo2-associated protein. Notably, Piezo2 accumulates at the apical surface of hair cells near the longest stereocilia and its specific subcellular distribution might contribute to regulation by Ca^{2+}, for example by affecting insertion of Piezo2 into the membrane. Such Ca^{2+} dependence may not be easily recapitulated in a heterologous system.

Previous studies identified stretch activated ion channels in the lateral membrane of hair cell[46-48]. We consider it unlikely that Piezo2 is the ion channel responsible for the reported currents. We detected little if any Piezo2 in the lateral membrane of hair cells and the properties of the reported channels are inconsistent with the properties of Piezo2. One study

reported a stretch-activated channel that is a potassium channel[47], while a second study reported a channel that is permeable to cations and anions[48]. A third study identified two types of stretch-activated ion channels, one with a voltage dependence inconsistent with the properties of Piezo2 and a second channel that is likely a potassium channel[46].

The ion channel carrying the reverse-polarity current is activated by disruptions of the sensory transduction machinery and by disruption of the sensory epithelium. The localization of Piezo2 at the apical surface of hair cells near junctional complexes between hair cells and support cells is intriguing. Perhaps, Piezo2 is critical to sense mechanical forces across the sensory epithelium that depends on adhesive contacts between hair cells and support cells. This might help to coordinate the maturation of the exquisitely organized sensory epithelium with the maturation of the sensory transduction machinery. It might also facilitate coordination or repair processes that are activated following pathological disruption of the sensory epithelium. In this regard it is notable that Piezo1 and Piezo2 have been implicated in the mechanical injury response in cartilage[49]. While speculative, it is also interesting to consider that Piezo2 might serve as a backup to maintain residual drive for electromotility when hair bundles are damaged. As such, dual channel specialization in OHCs might be viewed as a safeguard mechanism in situations of hair cell damage.

METHODS

Ethic statement

IACUC Institutional Review Boards at the Scripps Research Institute, Stanford Medical School and the University of Wisconsin approved all animal procedures.

Mouse strains, ABR and DPOAE measurement

Piezo1-flox, *Piezo2-flox*, *Pax2-Cre*, *Piezo1-null*, *Piezo2-null* mice and *Tmc1/Tmc2* double mutants were maintained on a C57BL/6 background and have been described previously[16, 28, 30, 43, 50, 51]. Animals of both sexes were used in experiments. Animals were maintained (3/cage) on a 12 h reverse light/dark cycle, and all behavioral and physiological tests were performed in the active (dark) phase. ABR and DPOAE measurements were carried out as described[52]. For DPOAE measurements, the cubic (2f1-f2) DPOAE thresholds were determined at a range of frequencies (8–32 kHz), evoked using two equal intensity primary stimuli about the test frequency, applied to the ear canal using two MF1 magnetic speakers coupled via an ER10B microphone probe (Etymotic Research, Elk Grove Village, IL). Stimuli were increased in intensity from 0 to 70 dB in 5 dB increments to establish thresholds.

Swimming test

To gauge effects of Piezo2 on vestibular function, animals were placed in an open field enclosure (50×40×13 cm) full of water and their spontaneous behavior videotaped and scored on the 4-point (0-3) swimming rating scale[31]. Both hind limbs were observed over a 1 min session for movements. Head position, tail propelling, body elongation, hind limb/tail coordination, and overall trunk stability were taken into account following the published procedure[31].

In situ Hybridization

In situ hybridization was carried out as described[53]. For in situ hybridization, two fragments of mPiezo1 cDNA (292-1054 bp and 5785-6796 bp of NM_001037298.1) and mPiezo2 cDNA (4781-5845 bp and 8229-9298 bp of NM_001039485) were sub-cloned and used to generate sense and antisense probes.

Scanning electron microscopy

Scanning electron microscopy was carried out as described[4]. Briefly, cochlear tissue was fixed and the TM was removed for hair cell scanning. Samples were dehydrated, processed to critical drying point, mounted, coated with iridium, and imaged.

Immunolocalization studies

For immunolocalization studies, the organ of Corti was fixed with 4% paraformaldehyde in PBS. After permeabilization and blocking with 5% BSA and 0.5% Triton X-100, samples were then incubate with primary antibody to Piezo2[23] (1:1000) and Alexa Fluor 586-phalloidin (1:800, ThermoFisher Scientific, Waltham, MA)[4, 5] and secondary antibodies (Anti-rabbit IgG, 1:2000, ThermoFisher Scientific). After rinsing in PBS, samples were cover-slipped with Vectashield. Labeled sections were imaged using a Nikon A1 Confocal Laser Microscope System (Tokyo, Japan). Specificity of the antibody was previously reported[23] and confirmed by comparing staining of tissue from wild-type and mutant animals.

Electrophysiology in hair cells

Mechanotransduction currents were recorded following our published procedure[4]. Cells were whole-cell patched for recording mechanotransduction currents at −70 mV holding potential with a patch clamp amplifier (EPC 10 USB, HEKA Electronics, Lambrecht/Pfalz, Germany, and Axopatch 200B, Molecular Devices, Sunnyvale, CA). For mechanical stimulation, hair bundles were deflected with a glass probe mounted on a piezoelectric stack actuator (P-885, Physik Instrument, Karlsruhe, Germany). The actuator was driven with voltage steps that were low-pass filtered at 10 KHz frequency to diminish the resonance of the piezo stack. Recording chamber was perfused artificial perilymph (in mM): 144 NaCl, 0.7 NaH_2PO_4, 5.8 KCl, 1.3 $CaCl_2$, 0.9 $MgCl_2$, 5.6 glucose, and 10 K-HEPES, pH 7.4. In some recordings, Ca^{2+} concentration was reduced to 0.02 mM. The patch pipette was filled with intracellular solution (140 mM KCl, 1 mM $MgCl_2$, 0.1 mM EGTA, 2 mM Mg-ATP, 0.3 mM Na-GTP and 10 mM K-HEPES, pH7.2). Cells were clamped at −70 mV. To record reverse polarity currents in OHCs, 5 mM BAPTA was added to the bath solution. The reverse polarity currents were elicited from OHCs using a fluid jet from a pipette (tip diameter of 10–15 μm). Sinusoidal force stimulus was applied to a 27-mm-diameter piezoelectric disc to produce fluid jet. The position of the pipette delivering the fluid jet was positioned at the modiolar side of the hair bundles and adjusted to elicit maximal MET currents. The sinusoids (40 Hz) was generated with Patchmaster 2.35 software (HEKA) or pClamp (Axopatch 200B) and filtered at 1.0 kHz with 900CT eight-pole Bessel filter (Frequency Devices, Ottawa, IL). Whole cell recordings were carried out and currents were sampled at 100 KHz with an EPC 10 USB patch-clamp amplifier or Axopatch 200B.

Composition of artifical perilymph was (in mM): 144 NaCl, 0.7 NaH_2PO_4, 5.8 KCl, 1.3 $CaCl_2$, 0.9 $MgCl_2$, 5.6 glucose, and 10 H-HEPES, pH 7.4. The patch pipette was filled with intracellular solution (140 mM KCl, 1 mM $MgCl_2$, 0.1 mM EGTA, 2 mM Mg-ATP, 0.3 mM Na-GTP and 10 mM H-HEPES, pH7.2). In some recordings, 1mM Ca^{2+} was added. Cells were clamped at −70 mV.

For measurements of transducer currents at high intracellular Ca^{2+}, we perfused cells with the following composition (mM): CsCl, 10 Tris phosphocreatine, 3 MgATP, 10 HEPES (pH 7.2) with 1 EGTA, 1 $CaCl_2$ or 2.5 $CaCl_2$, and CsCl concentrations of 135, 132 and 128 mM respectively.

Nonlinear capacitance (NLC) was measured by a two-sinusoidal method[54]with jClamp (SciSoftCo.,New Haven, CT) and fitted to the first derivative of a two-state Boltzmann function with SigmaPlot (San Jose, CA)[55]:

$$C_m = NLC + C_{lin} = Q_{max} * (ze/kT) * \exp(-ze(V_m - V_{pk})/kT) / (1 + \exp(-ze(V_m - V_{pk})/kT))^2 + C_{lin}$$

where Q_{max} is the maximum charge transferred, V_{pk} is the peak of NLC, z is the number of elementary charge (e), k is Boltzmann's constant, and T is the absolute temperature. Membrane potential (V_m) was corrected for electrode access resistance (Rs).

Transfection and electrophysiology in cell lines

HEK293 cells were directly purchased from ATCC (Manassas, VA) and were authenticated by STR analysis with AuthentiFiler PCR Amplication Kit (ThermoFisher Scientific). Cells were tested for mycoplasma on a weekly basis with mycoplasma kit (ThermoFisher Scientific). HEK293 cells were transiently transfected to express Piezo2-GFP[18] using Lipofectamine 2000 (ThermoFisher Scientific). 12 hours after transfection, cells were dissociated and plated onto poly-L-lysine-precoated coverslips and kept for another 15 hours in an incubator at 37°C before electrophysiological recording. Cells were whole-cell patched to record mechanically evoked currents at −70 mV using an Axopatch 200B (Molecular Devices, CA). Mechanical stimulation of the cell surface was achieved by a glass probe driven by piezo-electric crystal microstage (E625 Amplifier, Physik Instrument, Karlsruhe, Germany). Recording chamber was perfused (in mM): 127 NaCl, 3 KCl, 2.5 $CaCl_2$, 1 $MgCl_2$, 10 glucose, and 10 K-HEPES, pH 7.4. In some recordings, Ca^{2+} concentration was reduced to 0.02 mM. The patch pipette was filled with intracellular solution (133 mM CsCl, 1 mM $MgCl_2$, 5 mM EGTA, 10 mM $CaCl_2$, 4 mM Mg-ATP, 0.4 mM Na_2-GTP and 10 mM H-HEPES, pH7.3). Osmolarity, 295 mOsm.

Data Analysis and statistics

Data analysis was performed using Excel (Microsoft, Redmond, WA), OriginLab Northampton, MA), and MATLAB (MathWorks, Natick, MA). All data are mean ± SEM or percentage. Data collection was randomized. Some electrophysiological recordings were performed in blind in which genotyping were performed by another person after recordings. No statistical methods were used to pre-determine sample sizes but our sample size are similar to those reported in previous publications[4, 5, 17, 19, 37]. Data distribution was assumed

to be normal but this was not formally tested. We used the Mann-Whitney U-test or unpaired t-tests (two-tailed) to compared two groups. Paired t-tests were used to determine statistical significance between measurements in the same cohort. One-way ANOVA followed by Tukey's *post hoc* test were used to compared more than two groups. Percentage of cells or pups between different groups were analyzed with Fisher's exact tests (two groups) or Chi-Square tests (more than two groups). $P < 0.05$ was considered statistically significant. Student's two-tailed paired or unpaired *t* tests were used or different cohorts, respectively (*$p < 0.05$, **$p < 0.01$, ***$p < 0.001$). Detailed statistics for all experiments is provided in the figure legend and supplement checklist.

Supplementary Material

Refer to Web version on PubMed Central for supplementary material.

ACKNOWLEDGEMENT

This research was funded by NIDCD grants DC005965, DC007704, DC014713 (U. Müller); DC01362 (R. Fettiplace); NIDCR DEo22358 (A. Patapoutian); the Dorris Neuroscience Center; the Skaggs Institute for Chemical Biology (U. Müller). We like to thank S.-H. Woo and K. Nonomura for providing genetically modified mice for Piezo2 and for comments on the manuscript. A. Patapoutian is an investigator of the Howard Hughes Medical Institute. U. Müller is a Bloomberg Distinguished Professor.

REFERENCES

1. Gillespie PG, Muller U. Mechanotransduction by hair cells: models, molecules, and mechanisms. Cell. 2009; 139:33–44. [PubMed: 19804752]
2. Beurg M, Fettiplace R, Nam JH, Ricci AJ. Localization of inner hair cell mechanotransducer channels using high-speed calcium imaging. Nat Neurosci. 2009; 12:553–558. [PubMed: 19330002]
3. Kurima K, et al. TMC1 and TMC2 Localize at the Site of Mechanotransduction in Mammalian Inner Ear Hair Cell Stereocilia. Cell Rep. 2015; 12:1606–1617. [PubMed: 26321635]
4. Xiong W, et al. TMHS is an integral component of the mechanotransduction machinery of cochlear hair cells. Cell. 2012; 151:1283–1295. [PubMed: 23217710]
5. Zhao B, et al. TMIE is an essential component of the mechanotransduction machinery of cochlear hair cells. Neuron. 2014; 84:954–967. [PubMed: 25467981]
6. Labay V, Weichert RM, Makishima T, Griffith AJ. Topology of transmembrane channel-like gene 1 protein. Biochemistry. 2010; 49:8592–8598. [PubMed: 20672865]
7. Kawashima Y, et al. Mechanotransduction in mouse inner ear hair cells requires transmembrane channel-like genes. J Clin Invest. 2011; 121:4796–4809. [PubMed: 22105175]
8. Kim KX, Fettiplace R. Developmental changes in the cochlear hair cell mechanotransducer channel and their regulation by transmembrane channel-like proteins. J Gen Physiol. 2013; 141:141–148. [PubMed: 23277480]
9. Pan B, et al. TMC1 and TMC2 are components of the mechanotransduction channel in hair cells of the mammalian inner ear. Neuron. 2013; 79:504–515. [PubMed: 23871232]
10. Kim KX, et al. The role of transmembrane channel-like proteins in the operation of hair cell mechanotransducer channels. J Gen Physiol. 2013; 142:493–505. [PubMed: 24127526]
11. Kindt KS, Finch G, Nicolson T. Kinocilia mediate mechanosensitivity in developing zebrafish hair cells. Dev Cell. 2012; 23:329–341. [PubMed: 22898777]
12. Marcotti W, et al. Transduction without tip links in cochlear hair cells is mediated by ion channels with permeation properties distinct from those of the mechano-electrical transducer channel. The Journal of neuroscience : the official journal of the Society for Neuroscience. 2014; 34:5505–5514. [PubMed: 24741041]

13. Waguespack J, Salles FT, Kachar B, Ricci AJ. Stepwise morphological and functional maturation of mechanotransduction in rat outer hair cells. The Journal of neuroscience : the official journal of the Society for Neuroscience. 2007; 27:13890–13902. [PubMed: 18077701]
14. Alagramam KN, et al. Mutations in protocadherin 15 and cadherin 23 affect tip links and mechanotransduction in mammalian sensory hair cells. PLoS One. 2011; 6:e19183. [PubMed: 21532990]
15. Beurg M, Xiong W, Zhao B, Muller U, Fettiplace R. Subunit determination of the conductance of hair-cell mechanotransducer channels. Proc Natl Acad Sci U S A. 2015; 112:1589–1594. [PubMed: 25550511]
16. Beurg M, Kim KX, Fettiplace R. Conductance and block of hair-cell mechanotransducer channels in transmembrane channel-like protein mutants. J Gen Physiol. 2014; 144:55–69. [PubMed: 24981230]
17. Beurg M, Goldring AC, Fettiplace R. The effects of Tmc1 Beethoven mutation on mechanotransducer channel function in cochlear hair cells. J Gen Physiol. 2015; 146:233–243. [PubMed: 26324676]
18. Coste B, et al. Piezo1 and Piezo2 are essential components of distinct mechanically activated cation channels. Science. 2010; 330:55–60. [PubMed: 20813920]
19. Coste B, et al. Piezo proteins are pore-forming subunits of mechanically activated channels. Nature. 2012; 483:176–181. [PubMed: 22343900]
20. Honore E, Martins JR, Penton D, Patel A, Demolombe S. The Piezo Mechanosensitive Ion Channels: May the Force Be with You! Reviews of physiology, biochemistry and pharmacology. 2015; 169:25–41.
21. Schug N, et al. Differential expression of otoferlin in brain, vestibular system, immature and mature cochlea of the rat. Eur J Neurosci. 2006; 24:3372–3380. [PubMed: 17229086]
22. Yasunaga S, et al. A mutation in OTOF, encoding otoferlin, a FER-1-like protein, causes DFNB9, a nonsyndromic form of deafness. Nat Genet. 1999; 21:363–369. [PubMed: 10192385]
23. Woo SH, et al. Piezo2 is required for Merkel-cell mechanotransduction. Nature. 2014; 509:622–626. [PubMed: 24717433]
24. Madisen L, et al. A robust and high-throughput Cre reporting and characterization system for the whole mouse brain. Nat Neurosci. 2010; 13:133–140. [PubMed: 20023653]
25. Nornes HO, Dressler GR, Knapik EW, Deutsch U, Gruss P. Spatially and temporally restricted expression of Pax2 during murine neurogenesis. Development. 1990; 109:797–809. [PubMed: 1977575]
26. Groves AK, Bronner-Fraser M. Competence, specification and commitment in otic placode induction. Development. 2000; 127:3489–3499. [PubMed: 10903174]
27. Hutson MR, Lewis JE, Nguyen-Luu D, Lindberg KH, Barald KF. Expression of Pax2 and patterning of the chick inner ear. J Neurocytol. 1999; 28:795–807. [PubMed: 10900085]
28. Ohyama T, Groves AK. Generation of Pax2-Cre mice by modification of a Pax2 bacterial artificial chromosome. Genesis. 2004; 38:195–199. [PubMed: 15083520]
29. Rowitch DH, McMahon AP. Pax-2 expression in the murine neural plate precedes and encompasses the expression domains of Wnt-1 and En-1. Mech Dev. 1995; 52:3–8. [PubMed: 7577673]
30. Ranade SS, et al. Piezo1, a mechanically activated ion channel, is required for vascular development in mice. Proc Natl Acad Sci U S A. 2014; 111:10347–10352. [PubMed: 24958852]
31. Hardisty-Hughes RE, Parker A, Brown SD. A hearing and vestibular phenotyping pipeline to identify mouse mutants with hearing impairment. Nat Protoc. 2010; 5:177–190. [PubMed: 20057387]
32. Ashmore J. Cochlear outer hair cell motility. Physiol Rev. 2008; 88:173–210. [PubMed: 18195086]
33. Fettiplace R. Active hair bundle movements in auditory hair cells. J Physiol. 2006; 576:29–36. [PubMed: 16887874]
34. Ashmore JF. Forward and reverse transduction in the mammalian cochlea. Neuroscience research. Supplement : the official journal of the Japan Neuroscience Society. 1990; 12:S39–50. [PubMed: 2243636]

35. Santos-Sacchi J. Reversible inhibition of voltage-dependent outer hair cell motility and capacitance. The Journal of neuroscience : the official journal of the Society for Neuroscience. 1991; 11:3096–3110. [PubMed: 1941076]
36. Grillet N, et al. Harmonin mutations cause mechanotransduction defects in cochlear hair cells. Neuron. 2009; 62:375–387. [PubMed: 19447093]
37. Beurg M, Goldring AC, Ricci AJ, Fettiplace R. Development and localization of reverse-polarity mechanotransducer channels in cochlear hair cells. Proc Natl Acad Sci U S A. 2016; 113:6767–6772. [PubMed: 27162344]
38. Beurg M, Nam JH, Chen Q, Fettiplace R. Calcium balance and mechanotransduction in rat cochlear hair cells. J Neurophysiol. 2010; 104:18–34. [PubMed: 20427623]
39. Corey DP, Hudspeth AJ. Kinetics of the receptor current in bullfrog saccular hair cells. The Journal of neuroscience : the official journal of the Society for Neuroscience. 1983; 3:962–976. [PubMed: 6601694]
40. Lumpkin EA, Hudspeth AJ. Detection of Ca2+ entry through mechanosensitive channels localizes the site of mechanoelectrical transduction in hair cells. Proc Natl Acad Sci U S A. 1995; 92:10297–10301. [PubMed: 7479771]
41. Assad JA, Shepherd GM, Corey DP. Tip-link integrity and mechanical transduction in vertebrate hair cells. Neuron. 1991; 7:985–994. [PubMed: 1764247]
42. Hackney CM, Mahendrasingam S, Penn A, Fettiplace R. The concentrations of calcium buffering proteins in mammalian cochlear hair cells. The Journal of neuroscience : the official journal of the Society for Neuroscience. 2005; 25:7867–7875. [PubMed: 16120789]
43. Dubin AE, et al. Inflammatory signals enhance piezo2-mediated mechanosensitive currents. Cell Rep. 2012; 2:511–517. [PubMed: 22921401]
44. Lelli A, Asai Y, Forge A, Holt JR, Geleoc GS. Tonotopic gradient in the developmental acquisition of sensory transduction in outer hair cells of the mouse cochlea. J Neurophysiol. 2009; 101:2961–2973. [PubMed: 19339464]
45. Eijkelkamp N, et al. A role for Piezo2 in EPAC1-dependent mechanical allodynia. Nat Commun. 2013; 4:1682. [PubMed: 23575686]
46. Ding JP, Salvi RJ, Sachs F. Stretch-activated ion channels in guinea pig outer hair cells. Hear Res. 1991; 56:19–28. [PubMed: 1722801]
47. Iwasa KH, Li MX, Jia M, Kachar B. Stretch sensitivity of the lateral wall of the auditory outer hair cell from the guinea pig. Neurosci Lett. 1991; 133:171–174. [PubMed: 1726184]
48. Rybalchenko V, Santos-Sacchi J. Cl- flux through a non-selective, stretch-sensitive conductance influences the outer hair cell motor of the guinea-pig. J Physiol. 2003; 547:873–891. [PubMed: 12562920]
49. Lee W, et al. Synergy between Piezo1 and Piezo2 channels confers high-strain mechanosensitivity to articular cartilage. Proc Natl Acad Sci U S A. 2014; 111:E5114–5122. [PubMed: 25385580]

METHODS ONLY REFERENCES

50. Cahalan SM, et al. Piezo1 links mechanical forces to red blood cell volume. Elife. 2015; 4
51. Woo SH, et al. Piezo2 is the principal mechanotransduction channel for proprioception. Nat Neurosci. 2015; 18:1756–1762. [PubMed: 26551544]
52. Schwander M, et al. A forward genetics screen in mice identifies recessive deafness traits and reveals that pejvakin is essential for outer hair cell function. The Journal of neuroscience : the official journal of the Society for Neuroscience. 2007; 27:2163–2175. [PubMed: 17329413]
53. Grillet N, et al. Mutations in LOXHD1, an evolutionarily conserved stereociliary protein, disrupt hair cell function in mice and cause progressive hearing loss in humans. Am J Hum Genet. 2009; 85:328–337. [PubMed: 19732867]
54. Beurg M, Tan X, Fettiplace R. A prestin motor in chicken auditory hair cells: active force generation in a nonmammalian species. Neuron. 2013; 79:69–81. [PubMed: 23746629]
55. Zhu Y, et al. Active cochlear amplification is dependent on supporting cell gap junctions. Nat Commun. 2013; 4:1786. [PubMed: 23653198]

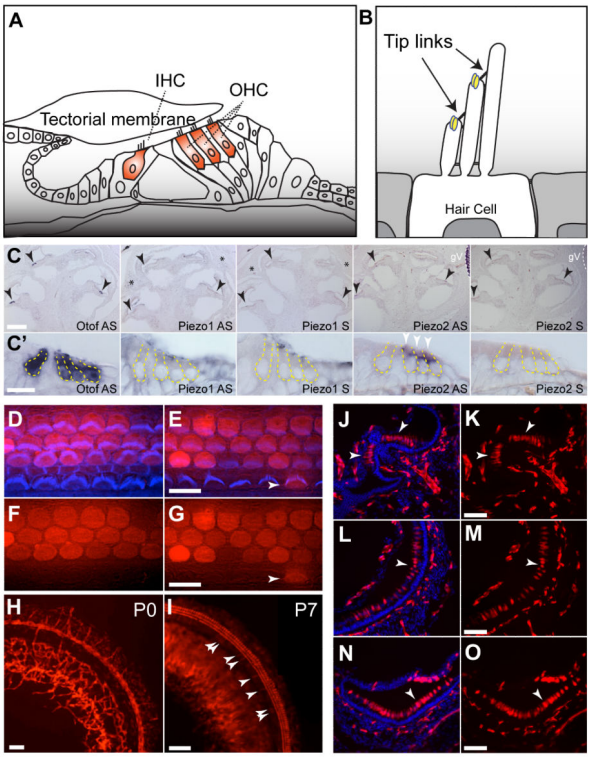

Fig. 1. Expression of Piezo1 and Piezo2 in the inner ear

(A) Diagram of the organ or Corti highlighting inner hair cells (IHCs) and outer hair cells (OHCs). (B) Diagram of a cochlear hair cell showing the stereocilia and part of the cell body. Linkages between stereocilia are highlighted. (C and C') In situ hybridization was carried out on cochlear sections at P1 with probes for otoferlin, Piezo1 and Piezo2 (AS, antisense probe; S, sense control probe). Arrowheads highlight OHCs expressing Piezo2 mRNA. gV (dashed white line) indicates staining of trigeminal sensory ganglia. (D-I) *Piezo2-Cre* mice were crossed with *Ai9* reporter mice, which contain a Cre-inducible td-Tomato transgene. td-Tomato fluorescence was visualized in cochlear whole mounts at the indicated age. Note expression in OHCs with occasional expression in IHCs (arrows in E,G,I). Blood vessels also expressed td-Tomato (H, I). In (D,E) phalloidin is in blue. (J-O) Vestibular whole mounts at the indicated age revealed td-Tomato expression in hair cells (arrow-heads) and in blood vessels. All experiments were repeated for at least 3 times, and at least 10 images were collected for each independent experiment. Phalloidin is in blue. Scale bars: (C) upper panel 200 μm, lower panel 20 μm; (D-G) 20 μm; (H-I) 100 μm; (J-O) 100 μm.

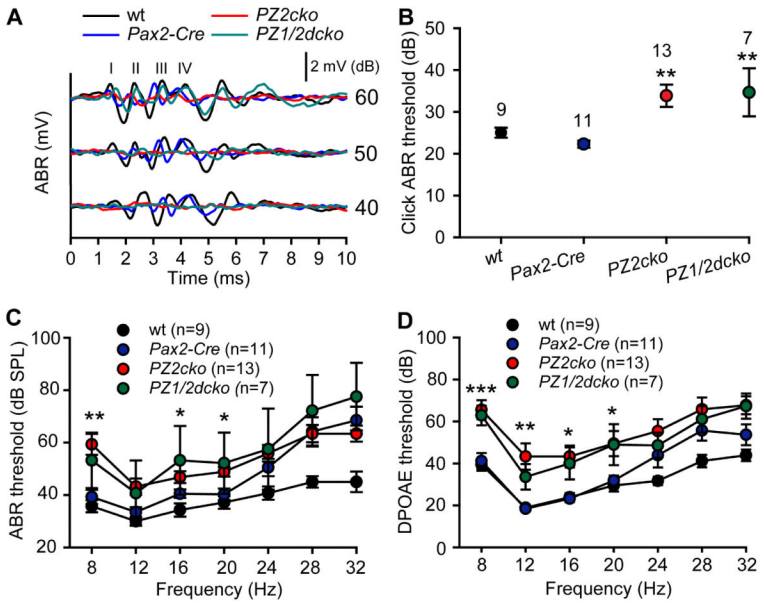

Fig. 2. Analysis of hearing function

(A) Representative ABR traces to click stimuli in the indicated control and mutant mice at 8 weeks of age. (B) Statistical results of ABR thresholds to click stimuli obtained similar data as shown in (A) at 8 weeks of age (mean ± standard error of the mean (SE); one-way ANOVA, **P = 0.005, F(3,36) = 5.07). The number of tested animals is indicated in the panel. (C) ABR thresholds to pure tones at 8 weeks of age (mean ± SE; one-way ANOVA test among *Pax2-Cre*, *PZ2cko*, and *PZ1/2dcko* groups: 8 Hz, **P = 0.007, F(2,28) = 5.858; 12 Hz, P = 0.187, F(2,28) = 1.834; 16 Hz, *P = 0.039, F(2,28) = 3.64; 20 Hz, *P = 0.04, F(2,28) =3.63; 24 Hz, P = 0.455, F(2,28) = 0.811; 28 Hz, P = 0.353, F(2,28) = 1.082; 32 Hz, P = 0.2, F(2,28) = 1.707). More than seven animals in each group were tested. (D) DPOAE thresholds at different frequencies in animals at 8 weeks of age (mean ± SE; one way ANOVA test among *Pax2-Cre*, *PZ2cko*, and *PZ1/2dcko* groups: 8 Hz, ***P < 0.001, F(2,28) = 9.808; 12 Hz, **P = 0.004, F(2,28) =6.611; 16 Hz, *P = 0.012, F(2,28) = 5.242; 20 Hz, *P = 0.047, F(2,28) =3.419; 24 Hz, P = 0.35, 1.091; 28 Hz, P =0.407, 0.927; 32 Hz, P = 0.083, F(2,28) = 2.717). More than seven animals in each group were tested.

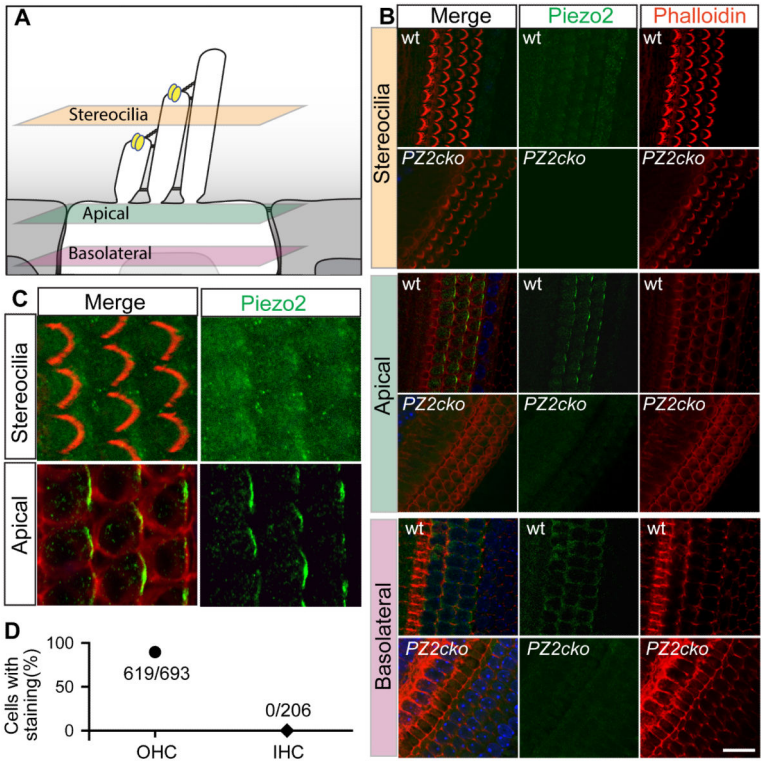

Fig. 3. Piezo2 localization in hair cells

(A) Diagram of a hair cells showing the approximate optical planes for imaging by confocal microscopy. (B,C) Cochlear whole mounts of wild-type mice (wt) and *Piezo2cko* mice (*PZ2cko*) at P5 were stained with phalloidin (red) and antibodies to Piezo2 (green). Note the prominent expression of PZ2 at the apical hair-cell surface near the base of stereocilia. In (C) the gain was drastically increased in optical sections through stereocilia stained for Piezo2. (D) Quantitative analysis of the Piezo2 staining in apical surface of OHCs and IHCs of wt mice similar as shown in (B) and (C). The numbers of analyzed hair cells is indicated. A least 10 images were collected from several independent experiment. Scale bars: 10 μm.

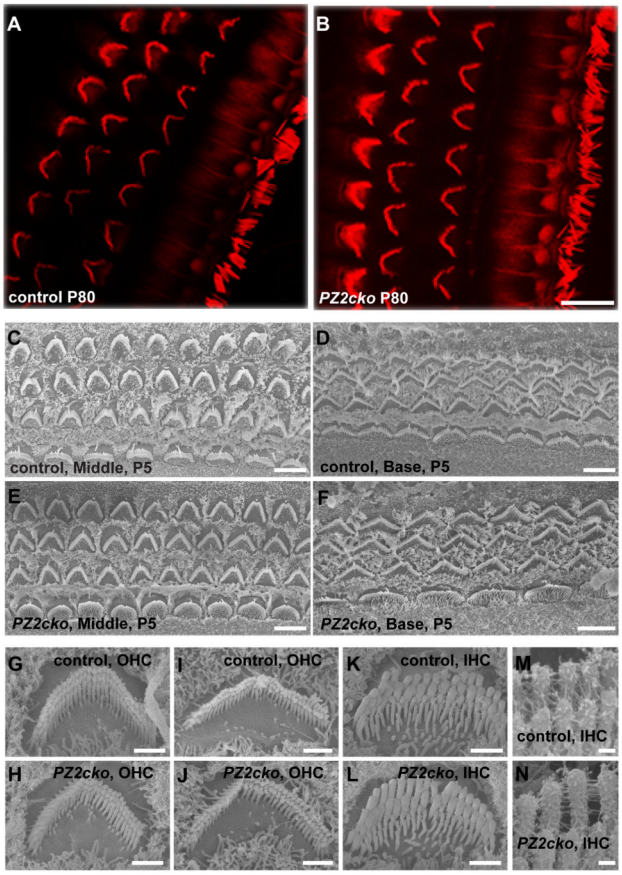

Fig. 4. Hair bundle morphology in *Piezo2cko* mice

(A,B) Analysis of the cochlea in P80 control and mutant animals by whole mount staining with phalloidin. There were no obvious defects in the patterning of the sensory epithelium or in the morphology of hair bundles of OHCs and IHCs. (C-N) Analysis of hair cells by SEM at P5. Hair cells in the middle part (C,E,G,H,K,L) and base (D,F,I,J) of the cochlea were imaged. (M,N) Higher magnification view of stereocilia of IHCs showing linkages between them. The experiments were carried out three times for P80 animals and twice for SEM. At least 5 images were collected from each independent experiment. Scale bars: (A,B) 10 μm; (C-F) 5 μm; (G-L) 1 μm; (M,N) 100 nm.

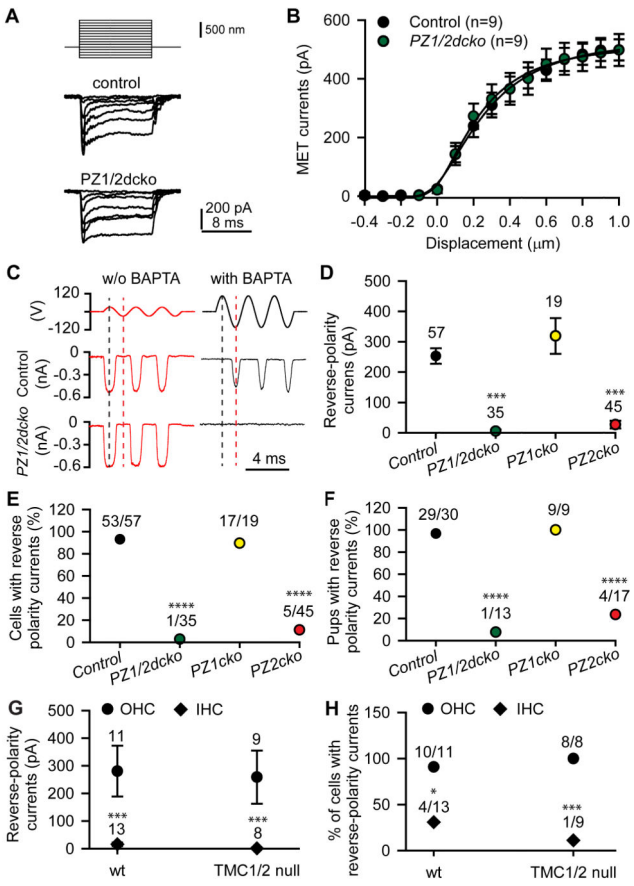

Figure 5. Analysis of forward-polarity and reverse-polarity currents

(A) Representative mechanotransduction currents in OHCs from control and *Piezo1/2dcko* mice (*PZ1/2dcko*) at P7 in response to a set of 10 msec hair bundle deflections ranging from −400 nm to 1000 nm (100 nm steps). (B) Current displacement plots obtained from similar data as shown in (A) (mean ± SEM; unpaired t-tests between control and *PZ1/2dcko* groups: −0.4 μm, P = 0.365, t(16) = 0.933; −0.3 μm, P = 0.053, t(16) = 2.089; −0.2 μm, P = 0.184, t(16) = 1.388; −0.1 μm, P = 0.884, t(16) =0.148; 0 μm, P = 0.797, t(16) = 0.261; 0.1 μm, P = 0.985, t(16) = 0.0186; 0.2 μm, P = 0.569, t(16) = 0.582; 0.3 μm, P = 0.767, t(16) = 0.302; 0.4 μm, P = 0.992, t(16) = 0.0101; 0.5 μm, P = 0.978, t(16) = 0.0283; 0.6 μm, P = 0.747, t(16) = 0.328; 0.7 μm, P = 0.971, t(16) =0.0365; 0.8 μm, P = 0.89, t(16) = 0.14; 0.9 μm, P = 0.9, 0.128; 1.0 μm, P = 0.995, t(16) = 0.0675. The number of tested animals is indicated in the panel. (C) Representative mechanotransduction currents in response to sinusoidal deflection of hair bundles at P5 for a wild-type C57BL/6 mouse and a *Piezo1/2dcko* mouse with and without BAPTA treatment. All recordings were from middle or apical OHCs at a holding potential of −70 mV; stimulus monitor, the driving voltage to the fluid jet, is shown at the top. A positive driving voltage denotes displacement toward the tallest edge of the hair bundle. In controls the response after BAPTA treatment occurs in the opposite phase (reverse-polarity) of the stimulus compared to the response prior to BAPTA treatment. Note that the reverse-polarity response is no longer detectable in *Piezo1/2dcko* mice. (D-F) Quantitative analysis of similar data as shown in (C). (G-H) Quantitative analysis of reverse-

polarity currents in IHCs from wt (after BAPTA treatment, P5) and *TMC1/2* double mutant (P6). Numbers of cells or pups for recordings are indicated. In (E, F, and H) the number of cells or pups that showed a response compared to the total number of cells or pups is indicated. Values in (D and G) are mean ± SEM. Values in (E, F, and H) are percentage. The genotype of pups in experiments (A-F) were revealed only after recordings were completed. One-way ANOVA for (D): ***P < 0.001, F(3,152) = 35.375. Chi-Square test for (E): ****P < 0.0001, X(3) = 114.5. Chi-Square test for (F): ****P < 0.0001, X(3) = 47.93. Mann-Whitney test for (G): wt, ***P < 0.001, U = 12.5; *Tmc1/2 null*, ***P < 0.001, U = 0. Fisher's exact test for (H): wt, *P = 0.045; *Tmc1/2 null*, ***P = 0.0004.

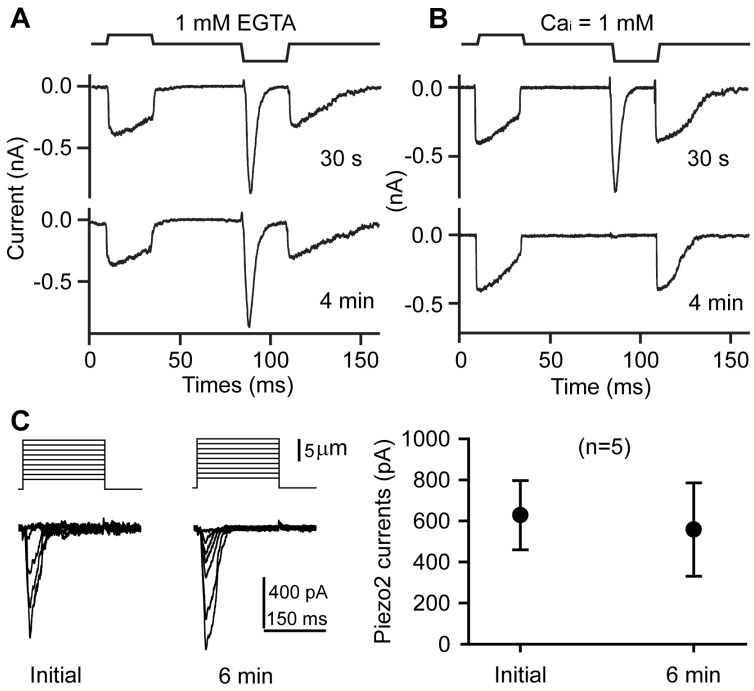

Figure 6. Effect of the intracellular Ca^{2+} concentration on reverse-polarity currents

(A) Normal and reverse-polarity currents recorded 30 sec after patch rupture (top) and 4 min after attaining whole cell recording. Internal solution containing 1 mM EGTA had no effect on either component. (B) Normal- and reverse-polarity currents 30 sec after patch rupture (top) and 4 min after attaining whole cell recording. Internal solution with 1 mM Ca^{2+} blocked reverse-polarity component but had no effect on normal MT currents. Similar effects of Ca^{2+} wash-in were seen in five OHCs with 1 mM Ca^{2+} in the pipette solution where the reverse-polarity current was 600 ± 130 pA immediately after attaining whole-cell and diminished after four minutes recording to 2 ± 0 pA but if EGTA was present in the patch-pipette solution, the reverse-polarity current was unaffected after 14 min of recording. (C) Piezo2-GFP was expressed in HEK cells and the cells were mechanically stimulated with a series of force steps to the cell surface via a piezo-driven glass probe. Currents were recorded with whole-cell voltage clamp recordings with a pipette solution containing up to 10 mM Ca^{2+}. Values are mean ± SEM, paired t-test: P = 0.811, t(8) = 0.247.

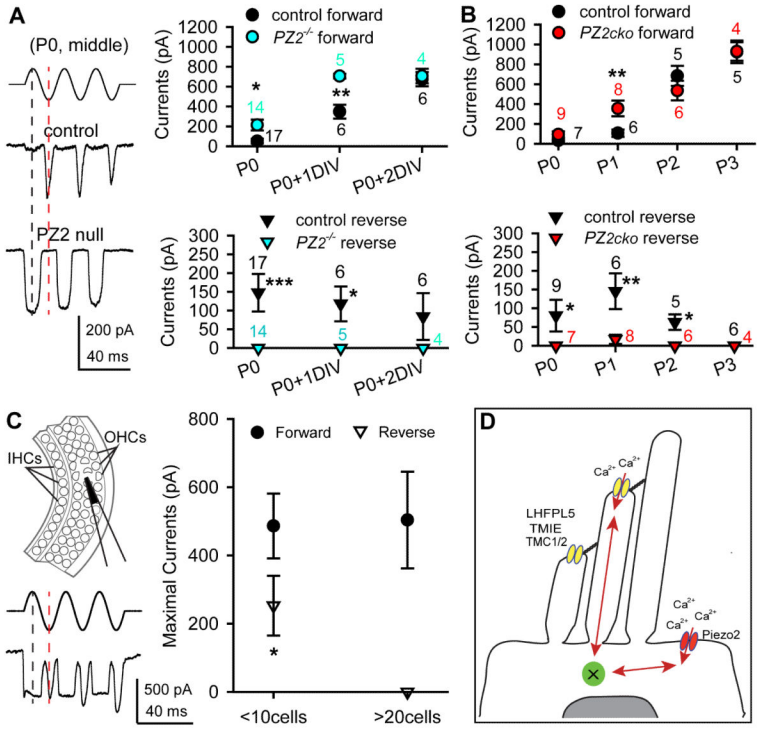

Figure 7. Maturation of mechanotransduction in OHCs from *Piezo2*-null mice and effects of mechanical disruption of the sensory epithlium on channel activity

(A) Cochlear explants were prepared from control and *Piezo2*-null mice at P0 and were cultured for the indicated time (DIV, day in vitro). Mechanotransduction currents were evoked by sinusoidal deflection of hair bundles with a fluid jet using OHCs at a similar position in the medial part of the cochlea in controls and mutants. On the left, typical recording are shown for an OHC from a wild-type and a *Piezo2*-null mouse. On the right, a quantitative analysis of the forward currents (upper pannel) and reverse-polarity currents (lower pannel) data similar as left traces is shown. The numbers of hair cells used for recordings are indicated. (B) Similar experiments as in (A) were performed on fresh cochlear explants from control and *Piezo2kco* mice from P0 to P3. Values are mean ± SEM. Mann-Whitney test between wt and *Piezo2* null for (A): P0 (forward currents), *P = 0.013, U = 57; P0+1DIV (forward currents), **P = 0.004, U = 0; P0+2DIV (forward currents), P = 0.762, U = 10; P0 (reverse currents), ***P < 0.001, U = 22.5; P0+1DIV (reverse currents), *P = 0.017, U =2.5; P0 + 2DIV (reverse currents), P = 0.476, U =8. Mann-Whitney test between wt and *Piezo2dcko* for (B): P0 (forward currents), P = 0.057, U = 13; P1 (forward currents), *P = 0.008, U = 4; P2 (forward currents), P = 0.247, U = 8; P3 (forward currents), P = 0.905, U =9; P0 (reverse currents), *P = 0.005, U = 9; P1 (reverse currents), *P = 0.013, U = 5; P2 (reverse currents), *P = 0.03, U = 3; P3 (reverse currents), P = 1, U = 10. The genotype of pups in (A,B) were revealed only after recordings were completed. (C) Left-upper diagram showing the experimental strategy to mechanically disrupt the sensory epithelium by insertion of a pipette. In the lower-left panel, representative mechanotransduction currents are shown that were evoked with a fluid jet after mechanical disruption of the sensory epithelium (P4). On the right, a quantitative analysis of the data is shown. Values are mean ± SEM. Mann-Whitney test between OHCs at different distance

from wound site: *P = 0.01, U = 0 for reverse-polarity currents and P = 0.257, U = 6.5 for forward-polarity currents. Cell number was used to indicate the distance between recorded cells and wound site. (D) Model showing the localization of the sensory transduction channel and the Piezo2-dependent channel in hair cells and their cross-regulation by Ca^{2+}. Both ion channels are permeable to Ca^{2+} and their activity is regulated by Ca^{2+}. Regulation of Piezo2 function by Ca^{2+} is likely indirect and might involve an intermediary protein (X) such as a kinase or phosphatase.